Hydrogeology Journal
https://doi.org/10.1007/s10040-021-02342-y

REPORT

Application of electrical resistivity to map the stratigraphy and salinity of fluvio-deltaic aquifers: case studies from Bangladesh that reveal benefits and pitfalls

Micaela N. Pedrazas[1] · M. Bayani Cardenas[1] · Alamgir Hosain[2] · Cansu Demir[1] · Kazi Matin Ahmed[3] · Syed Humayun Akhter[3] · Lichun Wang[4] · Saugata Datta[5] · Peter S. K. Knappett[6]

Received: 29 August 2020 / Accepted: 21 March 2021

Abstract

Fluvio-deltaic aquifers are the primary source of drinking water for the people of Bangladesh. Such aquifers, which comprise the Ganges-Brahmaputra-Meghna Delta, are hydrogeologically heterogeneous. Because of widespread groundwater quality issues in Bangladesh, it is crucial to know the hydrostratigraphic architecture and hydrochemistry, as some aquifer units are contaminated, whereas others are safe. Geophysical methods provide a potentially effective and noninvasive method for extensive characterization of these aquifers. This study applies and investigates the limitations of using electrical resistivity imaging (ERI) for mapping the hydrostratigraphy and salinity of an aquifer-aquitard system adjacent to the Meghna River. Some electrical resistivity (ER) sections showed excellent correlation between resistivity and grain size. These suggest that ERI is a powerful tool for mapping internal aquifer architecture and their boundaries with finer-grained aquitards which clearly appear as low-ER zones. However, in parts of some ER sections, variations in electrical properties were determined by porewater resistivity. In these cases, low ER was indicative of brine and did not indicate the presence of finer-grained materials such as silt or clay. Accordingly, the following hydrostratigraphic zones with different resistivities were detected: (1) aquifers saturated with fresh groundwater, (2) a regional silt/clay aquitard, and (3) a deeper brine-saturated formation. In addition, shallow silt/clay pockets were detected close to the river and below the vadose zone. ERI is thus a promising technique for mapping aquifers versus aquitards; however, the observations are easily confounded by porewater salinity. In such cases, borehole information and groundwater salinity measurements are necessary for ground-truthing.

Keywords Electrical resistivity · Bangladesh · Hydrostratigraphy · Geophysical methods · Groundwater exploration

Introduction

South and Southeast Asia, and in particular Bangladesh, rely heavily on groundwater as the main drinking water supply (~80%), and as a means of poverty alleviation through farmland irrigation (Zahid and Ahmed 2006). However, overexploitation of the Bengal Basin aquifers during the last decade has resulted in a reduction of groundwater storage by 32% between 2003 and 2013 (Khaki et al. 2018). Compounding this groundwater depletion, widespread arsenic (As) poisoning of shallow aquifers derived from the reduction of As-rich Fe-oxyhydroxides is well known in the region (Datta et al. 2011; Nickson et al. 1998). The challenge of identifying and solving these groundwater resource issues is bedeviled by the ubiquitous problem of aquifer heterogeneity. Preferential flow and fast flow paths for contaminant transport to deeper aquifers are present (Michael and Khan 2016), obscuring the

✉ Micaela N. Pedrazas
mpedrazash@utexas.edu

[1] Department of Geological Sciences, The University of Texas, Austin, TX, USA

[2] Department of Coastal Studies and Disaster Management, University of Barisal, Barisal, Bangladesh

[3] Department of Geology, University of Dhaka, Dhaka, Bangladesh

[4] Institute of Surface-Earth System Science, School of Earth System Science, Tianjin University, Tianjin, China

[5] Department of Geological Sciences, University of Texas, San Antonio, TX, USA

[6] Department of Geology and Geophysics, Texas A&M University, College Station, TX, USA

Published online: 08 April 2021

prediction of which aquifers are vulnerable to ingress of dissolved As through breaks in clay layers (Mozumder et al. 2020) or the in-situ release of As by reductive dissolution of iron oxides by dissolved organic carbon (DOC) drawn from clay layers under the influence of depressurization of low-As aquifers (Mihajlov et al. 2020). First-order information regarding sedimentary architecture such as the spatial extent and thickness of hydrogeologic units is necessary to mitigate contamination risks and resource issues. However, an in-depth understanding of the continuity of hydrostratigraphic units, connections with surface-water bodies, and porewater salinity distribution can be difficult to obtain.

There is a pressing need to advance the understanding of the fluvio-deltaic aquifer-aquitard system along the Meghna River in Bangladesh. Many villages are found along the banks of the Meghna. In Bangladesh, despite the relatively cheap cost of drilling wells by western standards, the expenses are still prohibitive for locals especially those relying on private wells for domestic water use. Hence, for the millions of privately owned wells, groundwater exploration is usually not exercised with extensive mapping. Direct observations made through drilling are sparse, expensive and provide only limited point observations of lithology and groundwater salinity.

Electrical resistivity imaging (ERI) is a cost-effective near-surface geophysical method that can image the electrical properties of aquifers and water stored within its pores (Daily et al. 1992). With ERI, an electrical current is injected into the subsurface using electrodes buried just beneath the surface. The voltaic response of the subsurface materials is then recorded by potential electrodes while the electrical current is active. The technique is useful for groundwater applications because the electrical resistivity of porous media is controlled by multiple geological and pore-fluid properties such as porosity, porewater salinity, fluid saturation, soil texture, overburden pressure, temperature, and electrical surface properties of the grain matrix (Cai et al. 2017; Loke 2011). In shallow fluvio-deltaic aquifers, below the water table, where the overburden pressure and water saturation are more or less static, ERI is particularly sensitive to the resistivity contrasts between aquifers (relatively coarser sediment) and aquitards (relatively finer sediment) as well as porewater resistivity. Thus, ERI can potentially discriminate between freshwater aquifers, brine saturated aquifers, and aquitards. Under optimal conditions, ERI can possibly map subunits with different textures and thus hydrologic properties within aquifers.

In Bangladesh, a few studies have determined empirical relationships between bulk electrical resistivity and solute concentrations and geotechnical properties, as well as qualitative relationships between lithology and resistivity (Hossain 2016; Kabir et al. 2011; Woobaidullah et al. 2008). In other parts of the world, electrical resistivity has been used to delineate and monitor salt-water intrusion into freshwater aquifers (Adepelumi et al. 2009; De Franco et al. 2009; Nowroozi et al. 1999). This article reports on a few case studies which further reveal the benefits and pitfalls of ERI for integrated hydrostratigraphic and hydrochemical characterization of an aquifer-aquitard system along the Meghna River. The goal of this study is to illustrate how well (or not) ERI can work in the context of Bangladesh's fluvio-deltaic sedimentary aquifers in terms of its ability to distinguish aquifer physical and hydrochemical properties.

Background on the study area

The Bengal Basin encompassing major parts of Bangladesh and its neighboring regions is a result of the collision of India with Eurasia and concomitant filling of the basin with sediment derived from erosion of mountains and uplands and transported and deposited by the Ganges and Brahmaputra rivers to where the Bay of Bengal once existed (Najman et al. 2008). The end result is a thick sedimentary sequence that starts in the northern part of Bangladesh near Sylhet, where it is tens of meters thick, and reaches up to 20 km at the modern shoreward limit of the Ganges-Brahmaputra-Meghna River Delta complex (Alam et al. 2003). The Meghna River is the third largest river amongst the three in terms of annual volumetric discharge. It flows from north to south and merges with other major rivers before it empties into the Bay of Bengal.

The upper portions of the Bay of Bengal is filled with a Quaternary alluvial sequence deposited by the Ganges and Brahmaputra rivers (Wilson and Goodbred 2015). Broadly, there are two distinct aquifers within this sequence—a shallow aquifer comprised of fine sands that is sometimes capped by a grey colored clay/silt blanket, and a deeper aquifer comprised of medium to coarse sands. These two aquifers are separated by a relatively impermeable silt/clay layer (Islam et al. 2018) which is widely present across the Bengal Basin (McArthur et al. 2008) and near the Meghna River (Knappett et al. 2016; Mozumder et al. 2020).

The study focused on a site that is approximately 30 km east of the capital city of Dhaka. Areas within tens to hundreds of meters of the Meghna River were studied to map the structure of the shallow, high-As aquifer, and the continuity of the clay layer separating this aquifer from the underlying, generally low-As aquifer. Broadly, two study transects were established. The north and south transects are roughly 12 km apart along the river (Fig. 1). Electrical resistivity surveys were conducted in the north transect subsets in January 2016, including its west and east subset surveys which were on opposite banks of the south-flowing Meghna River. The surveys in the South transects were conducted in January 2020.

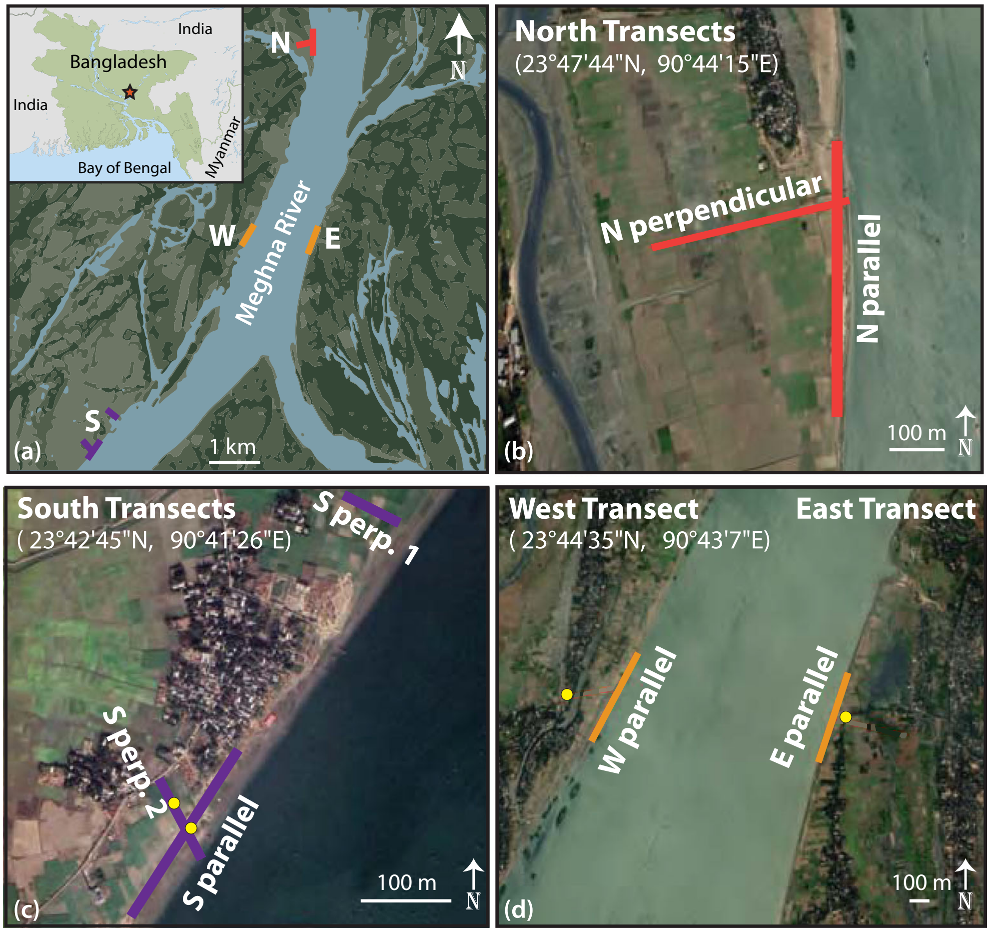

Fig. 1 **a** Overview of the study region and **b-d** locations of electrical resistivity imaging transects. The yellow circles denote boreholes where sediment grainsize and/or pore fluid resistivity were observed. The coordinates indicate the approximate center of each image. Images were taken from Google Earth

Methods

Electrical resistivity imaging and processing

An eight-channel ERI instrument (SuperSting R8, Advanced Geosciences, Inc.) with 84 electrodes was used for all surveys. When acquiring ERI surveys, there exists a trade-off between depth and resolution, which is controlled by the spacing between electrodes buried in the ground. Thus, different spacing arrangements were used for the surveys in order to acquire information at varying depths. In January 2016, four surveys 498-m long were acquired using the dipole-dipole array configuration and 6-m electrode spacing to investigate down to 100 m depth at the north, east and west study transects. In January 2020, the dipole-dipole array configuration was used with 1.5 and 3-m electrode spacing to investigate the near-surface shallow aquifer at a higher resolution at the south study transects (Fig. 1). To further distinguish the individual surveys, they are referred to by appending to their locations, e.g., north vs. south, whether the transect is perpendicular or parallel to the river and a number when there is more than one. A final name for the example is "South Perpendicular 1". This identification convention is followed throughout the article. The individual transects are shown in Fig. 1.

The ER data were processed and inverted using RES2DINV version 4.9.11 (Loke 2006) to obtain a subsurface resistivity distribution tomogram. All data were inverted using the robust inversion constraint and the finite-element method to minimize the root-mean square error (RMSE) difference between the measured and modeled apparent resistivity values. The robust inversion constraint was chosen to better resolve the expected presence of sand/silt (aquifer/aquitard) contacts. The parameters used in the inversion are presented in Table 1 and the apparent resistivity statistical information and RMS error for each survey is presented in Table 2. Additional post-processing steps, e.g., visualization, extraction of profiles, and statistical analyses, were conducted in the MATLAB program.

Direct observations of subsurface materials during well drilling: borehole data

Local drillers were hired to install deep piezometers and to obtain borehole cuttings. The drilling was performed using

Table 1 Parameters used for the inversion of electrical resistivity data. These are the options chosen when running when constructing and implementing the inversion in RES2DINV

Inversion parameter or property	Setting
Numerical model type	Finite-element
Inversion method	Robust inversion using L1 Norm
Robust data cut-off factor	0.05
Nodes	4
Initial damping factor	0.15
Minimum damping factor	0.02
V/H filter ratio	1
Model block discretization	Same width with reduced edge effects
Mesh size	Finest mesh grid size
Limit resistivities	None
Iterations	<6
Convergence limit for relative change in % RMS	5%

the local hand-flapper drilling method based on the application of suction and its release using the hand as a check valve to a PVC pipe (Horneman et al. 2004). As the pipe was lowered, sediment slurry was collected at every ~1.5-m intervals, and was immediately inspected for visual identification of the dominant grain size category. At each location, a cluster of three wells were drilled to different depths. Each well was screened at 1.5 m from the bottom. After well development and appropriate purging, the electrical conductivity of the groundwater was measured using a calibrated, handheld fluid electrical conductivity probe (YSI Professional Plus) at the boreholes from the east, west and south sites. Using a peristaltic pump, groundwater was actively pumped from the well into a small and continuously overflowing container wherein the probe was submerged. The nearest or overlapping borehole data were used in the interpretation for constraining the estimated bulk resistivity resulting from the processed ERI data. Figure 1 shows the spatial distribution of the borehole data.

Table 2 Apparent resistivity and inversion data. Outliers with apparent resistivity greater than 100,000 Ωm or lower than 0.01 Ωm were removed; the number of points removed are in parentheses. The minimum, maximum and mean apparent resistivity values are included for each survey. The *RMS* error for each inversion is also included. *Perp.* perpendicular

Survey	No. of measurements	RMS (%)	Min., Max., and Mean App. Res. (Ωm)
South Perp. 1	4,247 (4)	1.6	20.3, 1,903.3, 76.3
South Perp. 2	3,215 (0)	3.9	0.2, 1,355.4, 88.7
South Parallel	3,141 (21)	8.5	0.15, 3,192.9, 28.9
East Parallel	3,248 (1)	1.0	14.6, 115.6, 30.3
West Parallel	3,248 (2)	1.9	10.2, 66.9, 33.7
North Parallel	3,248 (0)	3.4	4.3, 122.0, 46.6
North Perp.	3,248 (0)	1.8	14.7, 823.2, 50.3

Calculation of theoretical bulk resistivity

Results of ERI can be interpreted by calculating the expected theoretical values for specific combinations of sediment and porewater properties. These properties represent the hydrologic and hydrochemical properties of the aquifer. Archie's Law relates all these properties (Archie 1942). It is the petrophysical relationship between bulk resistivity (ρ_b), fluid resistivity (ρ_w), sediment porosity (ϕ), and fluid saturation (S_w):

$$\rho_b = a\phi^{-m} S_w^{-n} \rho_w \quad (1)$$

Thus, if the parameters in Archie's law are known, one can determine the expected ρ_b values. Archie's law can also be used in inverse applications, whereby, if the ρ_b is known, e.g., from inverted ERI data (or ER tomograms), one could potentially determine any one of the parameters in Archie's law if the others are known or sufficiently constrained. In this study, expected ρ_b values were calculated and qualitatively compared with the observations. The following assumptions were considered: (1) the tortuosity factor $a=\phi^{1/2}$ (Bruggeman 1935); (2) the sediment is fully saturated below the water table (S_w): =1; the water table is typically no deeper than 2-3 m in the study transects); (3) the fluid resistivity (ρ_w) at discrete groundwater sampling depths is known following measurements; (4) the cementation factor $m = 1.983$ (Pearson et al. 1983); and finally, (5) porosity ϕ was assessed from the minimum for unconsolidated sand and gravel (20%) and the maximum for clay (60%) following typical values these sediment (Fetter 1994).

The classical Archie's law provides preliminary theoretical estimates of ρ_b. It ignores electrical conduction through the solid surface of the matrix and assumes current mainly passes through the fluid. Grain surface conduction of electrical currents may be important when clay minerals are present (Wang and Revil 2020; Cai et al. 2017; Glover et al. 2000; Waxman and Smits 1968).

Results and discussion

Shallow ER surveys: south transects

The south transects imaged down to ~30 m for the river-perpendicular surveys and to 50 m for the river-parallel survey (Fig. 2b). For the perpendicular surveys, away from the river and at higher elevation, there is a 2-m-thick very resistive (>316 Ωm) zone. This corresponds to the vadose zone. All transects showed a similar subsurface general resistivity distribution trend, which can be seen from vertical profiles of resistivity extracted from the middle of each tomogram (Fig. 2a). From top to bottom, there were five distinct resistivity zones: (1) a resistive (>75 Ωm) but heterogeneous ~2.5-m-thick zone spanning across the top of the survey transects, (2) an intermediate conductive zone (>31.6 and <75 Ωm) of approximately 6 m in thickness, (3) a 12-m-thick resistive layer that becomes most resistive at its vertical center, (4) a ~4-m-thick gradually changing resistive layer ranging from a high of ~90 Ωm at approximately 20 m depth to <30 Ωm below 24 m, and a (5) homogeneous low resistivity zone that continually decreased in resistivity with depth. The southern transects did not image the base of the least resistive bottom material. There were pockets of less resistive sediment within the intermediate resistive layer predominantly below the vadose zone and closest to the river.

Deep ER surveys: north, west, and east transects

The north, west and east transects were imaged down to 100 m (Fig. 3b). The perpendicular north transect showed a 2-m-thick very resistive vadose zone layer that extends for 60 m across the survey starting at about 60 m away from the river, similar to the South Perpendicular transects. All transects showed a similar general resistivity pattern illustrated further by the vertical resistivity profiles extracted from the middle of each survey, but with some exceptions (Fig. 3a). The uppermost 40 m of the deep surveys agreed with the results from the higher resolution shallow surveys with the exception of the West Parallel survey. In the latter's case, there were more conductive materials in the top 10 m. In the north transects, it became slightly more resistive with depth below 40 m, whereas within the West Parallel transect, the resistivity was constantly at 31.6 Ωm down to 80 m and then it became slightly more conductive deeper. The East Parallel survey results differed markedly from the rest; there was a very conductive layer below 40 m down to 100 m in the east transect.

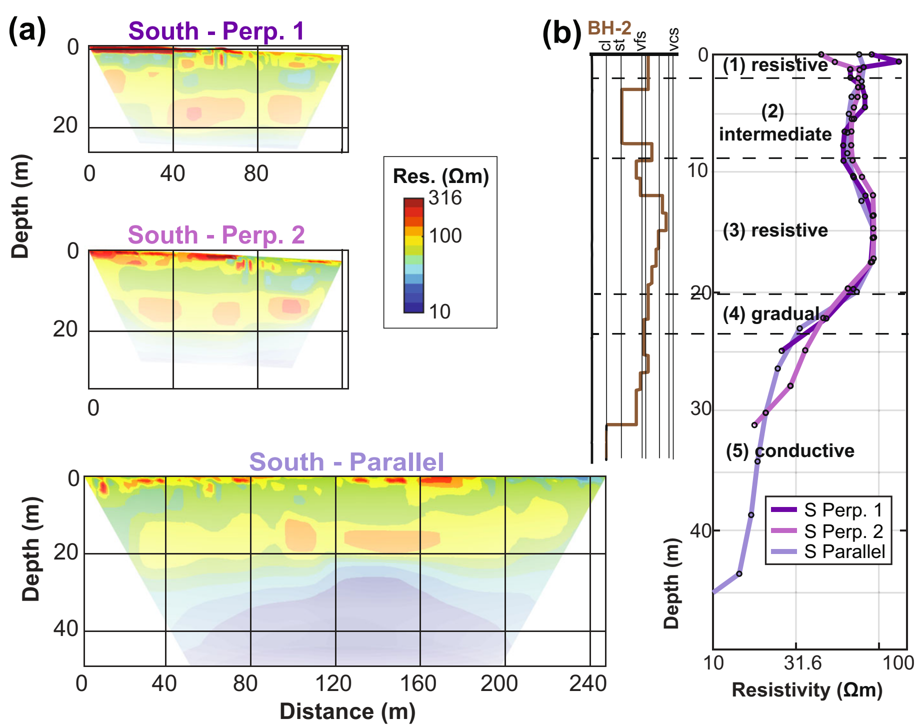

Fig. 2 **a** Resulting electrical resistivity tomograms and comparison with borehole data from the south transects. **b** Grainsize for cuttings from a nearby borehole (BH-2) and vertical resistivity profiles extracted from the middle of each resistivity survey (right). The grainsize categories are clay, silt, and very fine to coarse sand from left to right, respectively (**b**). The transparency of the tomograms reflects the model resolution decreasing with depth

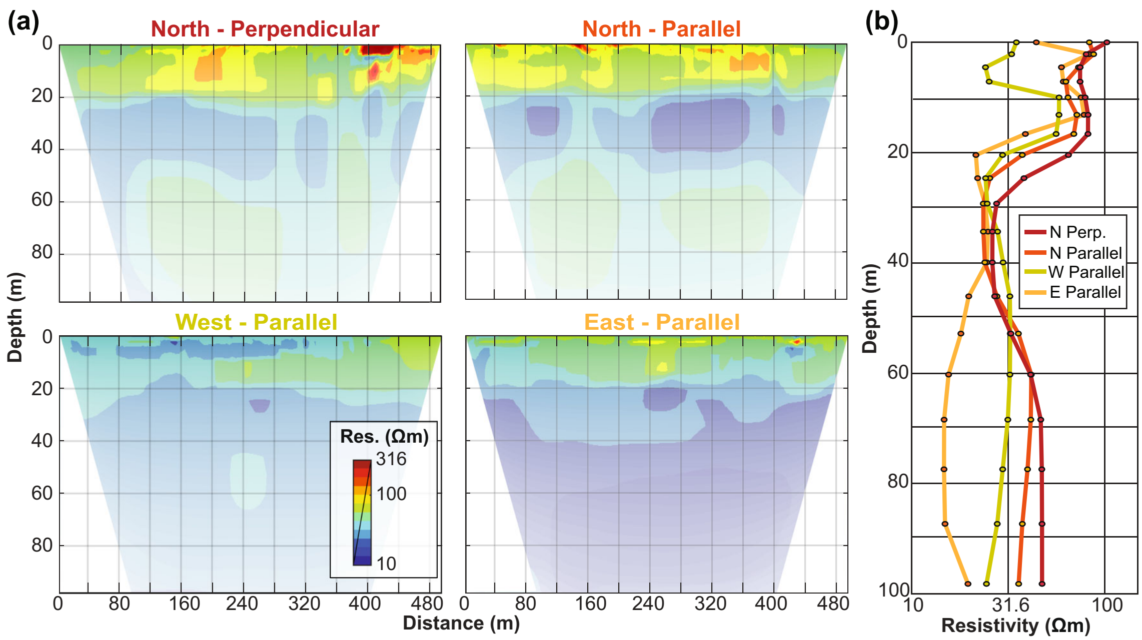

Fig. 3 **a** Electrical resistivity tomograms and **b** vertical profiles extracted from the middle of each survey shown down to their full depth extent for the north, west, and east transects. The locations of the transects are shown in Fig. 1b,d. The transparency of the tomograms reflects the model resolution decreasing with depth

Vertical distribution of fluid resistivity from well sampling

There were obvious variations in salinity within and across borehole locations. The east borehole (Fig. 4a) showed systematic increase in salinity with depth, with the pore fluid becoming very conductive (~5 Ωm or 2,108 µS/cm) down to about 70 m; yet, borehole cuttings did not indicate the presence of clay at any depths at which fluid resistivity was assessed. The west borehole showed moderate salinity variations with depth (Fig. 4b), increasing in resistivity by 6 Ωm at 46 m depth and then decreasing slightly by 2 Ωm at 61 m where clay cuttings were observed. The shallower south boreholes showed hardly any salinity variations with depth, with

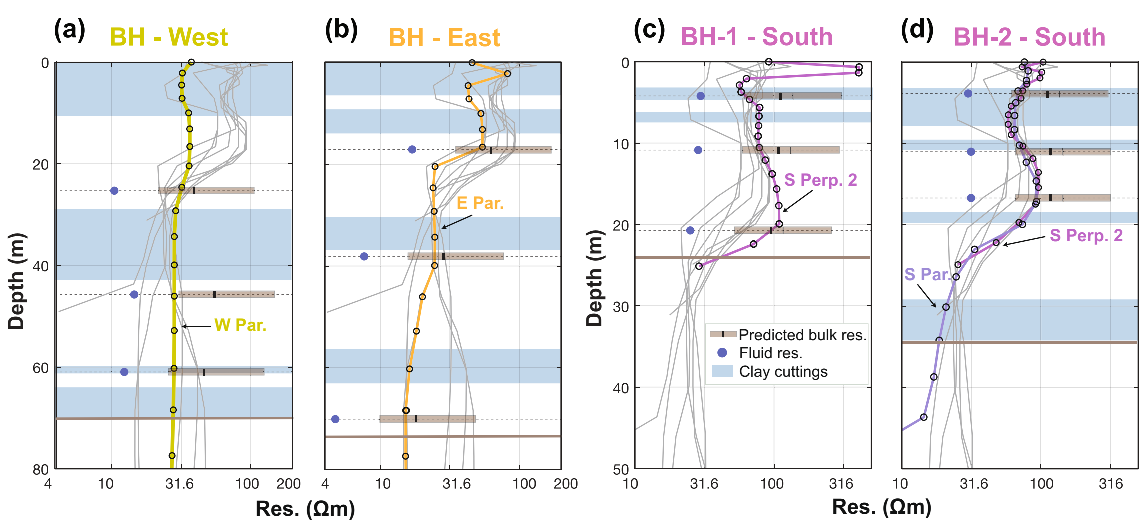

Fig. 4 Comparison of extracted vertical bulk electrical resistivity (ER) profiles from the tomograms with measured pore fluid resistivity and predicted bulk resistivity. A series of vertical ER profiles taken at equal horizontal distances across the tomograms are denoted by gray lines whereas the profile closest to the borehole (BH) is colored. The predicted bulk resistivity range, calculated using Archie's Law, is indicated by the brown bar with the median value denoted by the bold line. A porosity range of 20–60% and the measured fluid resistivity (blue circles) were assumed. Intervals with sediment finer than fine sand (i.e., very fine sand, silt and clay) are highlighted by the light blue shaded boxes. The borehole locations are shown in Fig. 1. BH-1 and BH-2 are along the South Perpendicular 2 transect, with BH-1 to the west. The water table is no deeper than 2 m below ground surface

fluid resistivity remaining at approximately 30 Ωm throughout the vertical profile even though clay cuttings were present at some depths where fluid resistivity was assessed (Fig. 4c,d).

Grainsize and lithological variations

Detailed lithology was logged during drilling only in the south transects where cuttings in the form of a sediment slurry were retrieved and visually assessed for grainsize at the site itself. There were two boreholes co-located along the South Perpendicular 2 survey line (BH-1 and BH-2), with the deeper of these two (BH-2) located at the intersections between the South Perpendicular 2 and South Parallel surveys (Fig. 1c). There is a general agreement between coarser grainsize and higher resistivity values. The grainsize log, when overlaid on top of the south tomograms, shows agreement of depth intervals with coarser grain size and higher resistivity values (Fig. 5). Furthermore, the combination of the tomograms (Fig. 5c) shows consistency across the different neighboring or overlapping transects, and thus continuity of the different zones. Cuttings from the other boreholes (east and west) were simply described as fine (silt/clay) or coarse materials (sand). The results of this binary description are shown in Fig. 4.

Constraining the inverted electrical resistivity tomograms with fluid resistivity and grainsize information

The combination of some fluid resistivity measurements and borehole lithology allows for constraining the ER tomograms. To analyze the relationship between grainsize and resistivity, vertical resistivity profiles were extracted from the tomograms at the borehole locations. These resistivity values were paired with the grainsize groups observed at their corresponding depths (Fig. 5). The groups are: (1) clay, (2) silt to very fine sand, (3) fine to medium sand, and (4) coarse to very coarse sand. A statistical comparison was then performed to determine if each grainsize group has a unique resistivity signature. Given the low sample numbers, a t-test statistic was used to evaluate if the groups had different means relative to each other. The t-test *p*-values (the probability of concluding that the groups have different means when they do not) showed that all the groups have different means at a 10% significance level ($p < 0.10$) and that almost all groups are also differentiable at the 5% significance level ($p < 0.05$) (Table 3). The only exception is the marginally significant ($p = 0.054$) difference in resistivity values for fine/medium sand and coarse/very coarse. The ability to distinguish between unique grainsize groups is further illustrated when visually comparing the statistical distributions (histograms) of resistivity for each group through 'violin plots'. The distinction between the different groups is visually apparent (Fig. 6). This indicates that at the south transects ERI is able to constrain the texture of the aquifer sediment (stratigraphic architecture) and also helps in the detection of the aquitards. The aquitard, comprised of silt and then finally clay was clearly detected underlying the aquifer at approximately 20 m depth.

Archie's law was used to predict the expected bulk resistivity based on the observed lithology and fluid resistivity. The predicted values (shown as bars in Fig. 4) for the south transects (Fig. 4c,d) roughly overlap with those were

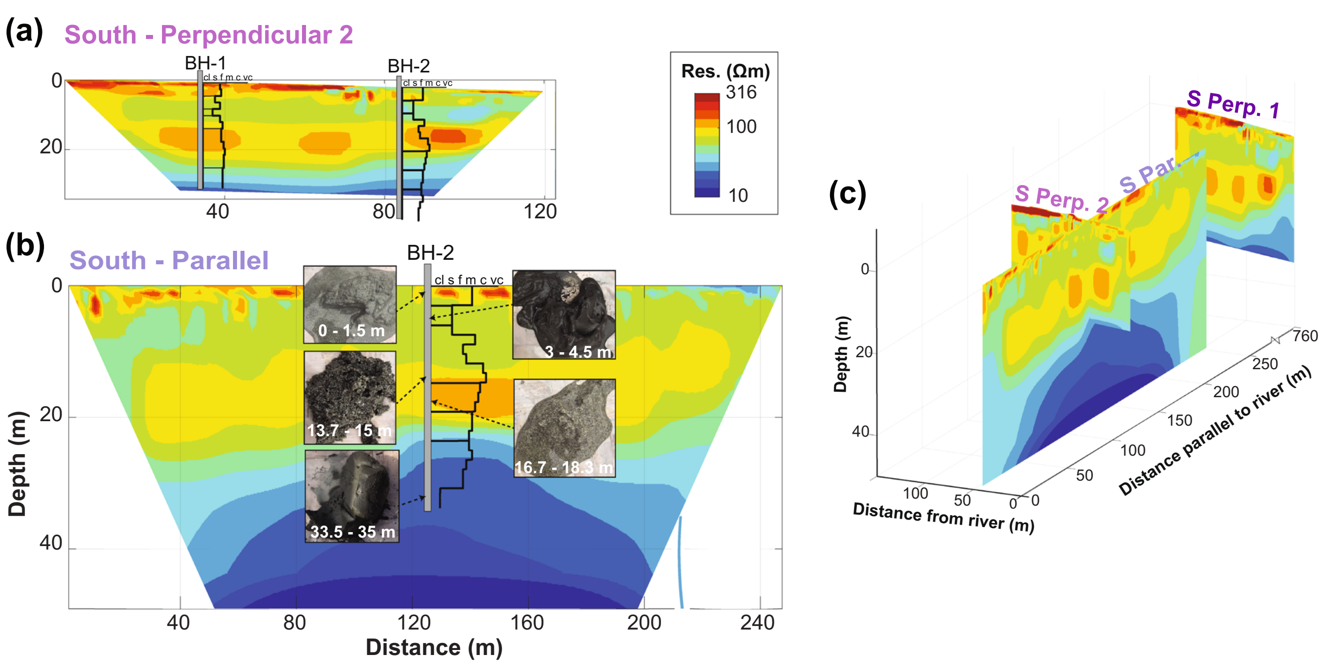

Fig. 5 **a** The superposed images of tomograms, borehole grainsize data and wet-sediment colors of core cuttings for the south transects. **b** The three-dimensional configuration and relationship of the tomograms

Table 3 Resulting p values of t-tests for comparing the resistivity of zones with different grainsize classes. The p value indicates the likelihood of accepting the hypothesis that the grain size groupings have different means when there is actually no difference. All p values are <0.1 (10% significance level) and most are <0.05 (5% significance level). The data used in the analysis correspond to those shown in Fig. 6

Grainsize class	Clay	Silt and very fine sand	Fine and medium sand	Coarse and very coarse sand
Clay	–	9.0×10^{-7}	7.5×10^{-9}	9.9×10^{-5}
Silt and very fine sand	9.0×10^{-7}	–	0.019	0.004
Fine and medium sand	7.5×10^{-9}	0.019	–	0.054
Coarse and very coarse sand	9.9×10^{-5}	0.004	0.054	–

observed in extracted vertical ER profiles; however, the resistivity values extracted from the tomograms tended to be on the lower range of if not lower than the predicted values. Similar comparisons between predicted and inverted tomogram profile values were observed for the west (Fig. 4a) and east (Fig. 4b) cases. The comparisons were least similar for the borehole close the west transect. This suggests that the porosity of the aquifer materials is smaller than the values used in Archie's law predictions, assuming that all other parameters were well constrained. However, this is unlikely given that the typical range was already used in the theoretical calculations. There are a few potential explanations—first, the resistivity of the aquifer materials is smaller, i.e., there are conductive minerals; second, the borehole is located approximately 200 m west of the ER transect and therefore may not be representative of the materials encountered within the coverage of the ER survey. Note that the borehole is offset from the ER transect (Fig. 1d). As such, some disagreement is not surprising

Further interpretation and limitations

The shallow surveys with shorter electrode spacing at the south site produce higher resolution resistivity tomograms.

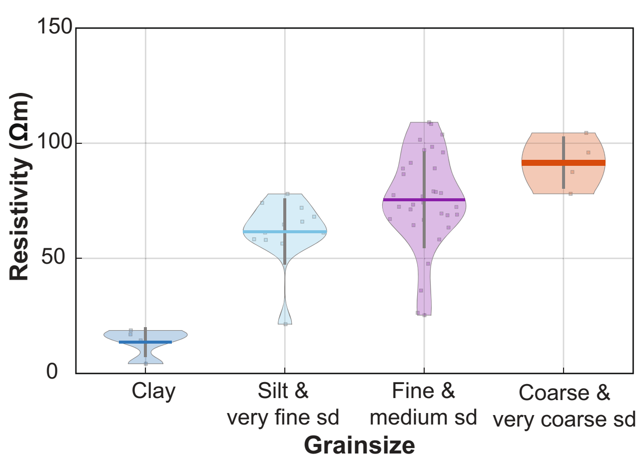

Fig. 6 Comparison of grainsize visually observed from borehole cuttings with bulk resistivity values for borehole locations for the south site. The comparison only includes observations below the water table. The violin plots show the relative density of data points for each grainsize grouping and highlight the mean (horizontal line) and interquartile range (vertical line). sd = sand

The south transects also exhibited minimum porewater salinity variation with depth than at the other sites (Fig. 4); thus, it was possible to correlate with and attribute the changes in resistivity to changes in sediment texture rather than fluid resistivity at the south transects. The lithological log at BH-2 correlated with the vertical resistivity profiles revealed that the first approximately 30 m from the top is comprised of sand (ranging from fine to medium sand) with a minor silt aquitard near the surface. This unconfined and semiconfined aquifer (owing to the minor intercalated silt) is underlain by a regional clay aquitard. Below this clay aquitard, the resistivity at the south site decreases until it reaches a value <10 Ωm at 50 m depth. The clay cuttings found at 31.5 m depth showed a resistivity of 20 Ωm; thus, a resistivity <10 Ωm may be indicative of brine-saturated sediment.

The deeper boreholes in the east and west sites reveal that the upper horizon of the clay aquitard is located at a depth of ~30 m and has a thickness of 6 m (east) and 12 m (west), followed by a deeper sandy aquifer and then another clay aquitard at a depth of ~60 m (Fig. 4a,b). For the north transects, where no borehole information is available, the transition between the shallow resistive layer and the conductive zone corresponded to the depth at which clay was found in the south transects (Fig. 2). According to the ER tomogram, below the clay aquitard of varying thickness, there is resistive sediment that is most likely the deeper sandy aquifer observed in the east and west boreholes. The conductive sediment below 30 m depth in the west and east tomograms is more difficult to interpret since in both sites the lithology log indicates a 20-m-thick deep sandy aquifer between 40 and 60 m depth, which is apparent in the north ER tomograms, but this depth interval manifests as a conductive zone in the west and east tomograms. Integration of the fluid resistivities into the analysis suggests that the higher electrical conductivity for the west and, especially, the east surveys, results from the higher porewater salinity. At 70 m depth, the east transect fluid resistivity reaches 4 Ωm, indicative of more saline porewater. It seems that the clay aquitard with resistivity ~30 Ωm is more resistive than brackish water-saturated sand <10 Ωm. However, in the deep zones, it is difficult to pinpoint the depth at which the conductive clay layer transitions to more saline water-saturated sand without additional evidence from borehole cuttings. Had the fluid resistivity in these conductive zones been unknown, this zone could have been interpreted as an aquitard if the lessons and resistivity-grainsize correlations from the south transects were extrapolated to this location.

The analysis and application of Archie's law here assumes that bulk resistivity variations due to the electrical properties of the solid matrix can be ignored. That is, there is no electrical conduction through the surfaces of the grains. This assumption is violated when substantial clay minerals are present (Wang and Revil 2020; Cai et al. 2017; Glover et al. 2000; Waxman and Smits 1968). Unfortunately, the lithologic characterization is not sufficient to quantify the clay content, let alone the cation exchange capacity of the clays and the bulk material in general which is necessary for constraining surface conduction (Wang and Revil 2020; Waxman and Smits 1968). Nonetheless, future studies of fluvio-deltaic aquifers with a mix of sand, silt, and clays should also consider petrophysical models which consider electrical conduction by the solid phase of the bulk sediment-water mixture, e.g., Glover et al. (2000) and Wang and Revil (2020).

Summary and conclusions

This study reports on hydrogeophysical mapping of two main aquifers vertically separated by a clay aquitard in the fluvio-deltaic sediment sequence next to the Meghna River in Bangladesh. Overall, the electrical resistivity tomograms indicate the prevalence of these three zones or hydrostratigraphic units. Going from top to bottom, these are: (1) a ~12-m thick freshwater-bearing coarse sand aquifer capped by a silt layer, (2) a ~10 m clay aquitard, and (3) a thick sandy aquifer with parts that are fresh and parts that are brine-saturated. When there is no strong variation in groundwater salinity, the electrical resistivity tomograms showed a strong correlation between resistivity and grainsize making electrical resistivity a powerful and efficient tool for hydrostratigraphic characterization. However, when substantial salinity variations are present, it is crucial to integrate fluid resistivity measurements to distinguish between the sediment and the porewater electrical signal. This is a major limitation to the broad application of the electrical resistivity imaging for physical mapping of aquifers. On the other hand, it also illustrates the potential to map hydrochemical variations at aquifer scales, but in this application, it is the sediment properties that need to be constrained.

Acknowledgements We thank Imtiaz Choudhury, Abu Saeed Arman, Mesbah Uddin Bhuiyan, Rajib Mozumder, Kimberley Rhodes and Kimberley Myers for assistance with field work. All geophysical data are available in Hydroshare (2021). We thank two anonymous reviewers for their comments.

Funding information MNP was supported by a fellowship from the Ivanhoe Foundation. This project was funded by the National Science Foundation (grants EAR-1852653, EAR-1940772 and EAR-1852652). Additional support was provided by the Geology Foundation of the University of Texas at Austin.

References

Adepelumi AA, Ako B, Ajayi T, Afolabi O, Omotoso E (2009) Delineation of saltwater intrusion into the freshwater aquifer of Lekki peninsula, Lagos, Nigeria. Environ Geol 56:927–933

Alam M, Alam MM, Curray JR, Chowdhury MLR, Gani MR (2003) An overview of the sedimentary geology of the Bengal Basin in relation to the regional tectonic framework and basin-fill history. Sediment Geol 155:179–208. https://doi.org/10.1016/S0037-0738(02)00180-X

Archie GE (1942) The electrical resistivity log as an aid in determining some reservoir characteristics. SPE-942054-G 146, pp 54-62. https://doi.org/10.2118/942054-G

Bruggeman DAG (1935) Berechnung verschiedener physikalischer Konstanten von heterogenen Substanzen: I. Dielektrizitätskonstanten und Leitfähigkeiten der Mischkörper aus isotropen Substanzen [Calculation of various physical constants of heterogeneous substances: I. dielectric constants and conductivities of mixed bodies made of isotropic substances]. Ann Phys 416:636–664. https://doi.org/10.1002/andp.19354160705

Cai JC, Wei W, Hu XY, Wood DA (2017) Electrical conductivity models in saturated porous media: a review. Earth Sci Rev 171:419–433. https://doi.org/10.1016/j.earscirev.2017.06.013

Daily W, Ramirez A, LaBrecque D, Nitao J (1992) Electrical resistivity tomography of vadose water movement. Water Resour Res 28: 1429–1442. https://doi.org/10.1029/91wr03087

Datta S, Neal AW, Mohajerin TJ, Ocheltree T, Rosenheim BE, White CD, Johannesson KH (2011) Perennial ponds are not an important source of water or dissolved organic matter to groundwaters with high arsenic concentrations in West Bengal, India. Geophys Res Lett 38. https://doi.org/10.1029/2011gl049301

De Franco R, Biella G, Tosi L, Teatini P, Lozej A, Chiozzotto B, Giada M, Rizzetto F, Claude C, Mayer A (2009) Monitoring the saltwater intrusion by time lapse electrical resistivity tomography: the Chioggia test site (Venice lagoon, Italy). J Appl Geophys 69:117–130

Fetter C (1994) Applied hydrogeology. Prentice Hall, Upper Saddle River, NJ, 691 pp

Glover PWJ, Hole MJ, Pous J (2000) A modified Archie's law for two conducting phases. Earth Planet Sci Lett 180:369–383

Horneman A, van Geen A, Kent DV, Mathe PE, Zheng Y, Dhar RK, O'Connell S, Hoque MA, Aziz Z, Shamsudduha M, Seddique AA, Ahmed KM (2004) Decoupling of as and Fe release to Bangladesh groundwater under reducing conditions, part I: evidence from sediment profiles. Geochim Cosmochim Acta 68:3459–3473. https://doi.org/10.1016/j.gca.2004.01.026

Hossain D (2016) Possibility of inferring water quality using DC electrical resistivity measurements: a case study of the Dupi Tila aquifer in Bangladesh. J Bangladesh Acad Sci 40:1–10

Hydroshare (2021) Application of electrical resistivity to map the stratigraphy and salinity of fluvio-deltaic aquifers: case studies from Bangladesh reveal benefits and pitfalls. https://doi.org/10.4211/hs.cf3c2633962b4121a231110d4be0d7a5

Islam M, Bashar K, Ahmed N, Rasul MG, Hossain S, Sarker MMR (2018) Hydrogeologic characteristics and groundwater potentiality of lower aquifer of Singair Upazila, Manikganj District, Bangladesh. J Bangladesh Acad Sci 42:25–40

Kabir AS, Hossain D, Abdullah R (2011) 2-D electrical imaging in some geotechnical investigation of Madhupur clays, Bangladesh. J Geol Soc India 77:73–81

Khaki M, Forootan E, Kuhn M, Awange J, Papa F, Shum CK (2018) A study of Bangladesh's sub-surface water storages using satellite products and data assimilation scheme. Sci Total Environ 625: 963–977. https://doi.org/10.1016/j.scitotenv.2017.12.289

Knappett P, Mailloux B, Choudhury I, Khan M, Michael H, Barua S, Mondal D, Steckler M, Akhter S, Ahmed K (2016) Vulnerability of low-arsenic aquifers to municipal pumping in Bangladesh. J Hydrol 539:674–686

Loke M (2006) RES2DINV ver. 3.55, rapid 2D resistivity and IP inversion using the least-squares method. Software manual 139, Geotomo Software, Penang, Malaysia

Loke M (2011) Electrical resistivity surveys and data interpretation. https://doi.org/10.1007/978-90-481-8702-7_46

McArthur J, Ravenscroft P, Banerjee D, Milsom J, Hudson-Edwards KA, Sengupta S, Bristow C, Sarkar A, Tonkin S, Purohit R (2008) How paleosols influence groundwater flow and arsenic pollution: a model from the Bengal Basin and its worldwide implication. Water Resour Res 44(11). https://doi.org/10.1029/2007WR006552

Michael HA, Khan MR (2016) Impacts of physical and chemical aquifer heterogeneity on basin-scale solute transport: vulnerability of deep groundwater to arsenic contamination in Bangladesh. Adv Water Resour 98:147–158. https://doi.org/10.1016/j.advwatres.2016.10.010

Mihajlov I, Mozumder MRH, Bostick BC, Stute M, Mailloux BJ, Knappett PS, Choudhury I, Ahmed KM, Schlosser P, van Geen A (2020) Arsenic contamination of Bangladesh aquifers exacerbated by clay layers. Nat Commun 11:1–9

Mozumder M, Michael H, Mihajlov I, Khan M, Knappett P, Bostick B, Mailloux B, Ahmed K, Choudhury I, Koffman T (2020) Origin of groundwater arsenic in a rural Pleistocene aquifer in Bangladesh depressurized by distal municipal pumping. Water Resour Res 56(7). https://doi.org/10.1029/2020WR027178

Najman Y, Bickle M, BouDagher-Fadel M, Carter A, Garzanti E, Paul M, Wijbrans J, Willett E, Oliver G, Parrish R, Akhter SH, Allen R, Ando S, Chisty E, Reisberg L, Vezzoli G (2008) The Paleogene record of Himalayan erosion: Bengal Basin, Bangladesh. Earth Planet Sci Lett 273:1–14. https://doi.org/10.1016/j.epsl.2008.04.028

Nickson R, McArthur J, Burgess W, Ahmed KM, Ravenscroft P, Rahmanñ M (1998) Arsenic poisoning of Bangladesh groundwater. Nature 395:338–338. https://doi.org/10.1038/26387

Nowroozi AA, Horrocks SB, Henderson P (1999) Saltwater intrusion into the freshwater aquifer in the eastern shore of Virginia: a reconnaissance electrical resistivity survey. J Appl Geophys 42:1–22. https://doi.org/10.1016/S0926-9851(99)00004-X

Pearson CF, Halleck PM, McGuire PL, Hermes R, Mathews M (1983) Natural gas hydrate deposits: a review of in situ properties. J Phys Chem 87:4180–4185. https://doi.org/10.1021/j100244a041

Wang H, Revil A (2020) Surface conduction model for fractal porous media. Geophys Res Lett 47(10). https://doi.org/10.1029/2020GL087553

Waxman MH, Smits LJM (1968) Electrical conductivities in oil-bearing shaly sands. Soc Pet Eng J 8:107–122

Wilson C, Goodbred S (2015) Construction and maintenance of the Ganges-Brahmaputra-Meghna Delta: linking process, morphology, and stratigraphy. Annu Rev Mar Sci 7. https://doi.org/10.1146/annurev-marine-010213-135032

Woobaidullah A, Chowdhury SH, Ahmed KM, Rahman MW, Arafin KS, Al-Ejaz O (2008) Geo-electric resistivity survey in the evaluation of hydrogeological condition in Haziganj Upazila, Chandpur District, Bangladesh. J Geol Soc India 72:753–763

Zahid A, Ahmed SRU (2006) Groundwater resources development in Bangladesh: contribution to irrigation for food security and constraints to sustainability. Groundw Gov Asia Ser 1:25–46